

Influence of Deoxyribose Group on Self-Assembly of Thymidine on Au(111)

Bing Yang,[†] Yeliang Wang,[†] Guo Li,[†] Huanyao Cun,[†] Ying Ma,[‡] Shixuan Du,[†] Mingchun Xu,[†] Yanlin Song,[‡] and H. -J. Gao^{*†}

Institute of Physics, Chinese Academy of Sciences, Beijing 100190, China, and Institute of Chemistry, Chinese Academy of Sciences, Beijing 100190, China

Received: July 22, 2009; Revised Manuscript Received: September 10, 2009

Using scanning tunneling microscopy (STM), we investigate the self-assembled structures and current-induced phase transition of one nucleoside species, thymidine (TD) on Au(111). By comparing the previous work on DNA nucleic acid base thymine on the same surface, we find that the deoxyribose groups of TD molecules remarkably enhance the intermolecular interaction and drive the formation of a dimer structure even at low temperature. At room temperature, TD molecules aggregate into well-ordered dimer islands. A two-dimensional (2D) gas-like phase of mobile TD molecules is also found surrounding the islands, and it can be transformed into the dimer structure. Furthermore, a new phase, a parallel-line structure, was observed gradually developing around the dimer domains under consecutive scanning. These molecular lines can be produced from both the gas-like phase and the dimer. First-principle calculations illustrate the optimized molecular superstructures in both phases.

Introduction

As one of the characteristics of matter, self-assembly is prevalent in many biological, chemical, and physical processes. Especially in biological systems, seemingly intricate and advanced life phenomena are supposed to be achieved by self-assembly of simple molecular building blocks, via functional groups and selective interactions. DNA is one of the most fundamental components of living cells with the ability to store and reproduce genetic information. DNA consists of phosphate, deoxyribose and nucleic acid bases (NB), leading to the double-helix structure.¹ The sequence of nucleic acid pairs (purines and pyrimidines) determines the genetic attribution of an organism. Therefore, it is of significance to study the self-assembly of NB molecules as a means to explore their inter- and intramolecular hydrogen-bonding properties and their ability to bind to amino acids,² constructing proteins and more complex biological systems. This will help to understand some fundamental biological processes, such as DNA translation and transcription, in order to reveal the mysteries of life's origin.

The unique capability of scanning probe microscopy (SPM) techniques³ provides the possibilities to directly resolve individual NB molecules in real space and investigate their interactions at the atomic/molecular level. Recently, self-assembled structures of NB molecules have been extensively studied by SPM techniques either on the solid/liquid interface^{4–15} or under UHV conditions.^{16–21} Also, theoretical calculations have been conducted to study the homopairing possibilities of these NB bases on metal surfaces^{22–26} and graphene.²⁷ For example, Xu et al.²⁸ recently reported on the self-assembled structures of thymine on Au(111). With increasing coverage,

they observed both dimer filaments and ordered dimer islands at room temperature (RT). By applying voltage pulses, these 2D islands can be disassembled into 1D filaments, which confirms the speculation of hierarchical thymine–thymine interactions. However, all previous works only focused on the nucleic acid bases without any terminal deoxyribose group. Therefore, investigations that reveal the role of the deoxyribose group are strongly needed for a better understanding of the interactions within DNA molecules.

In this letter, we employ thymidine (TD), one of the nucleoside molecules, which is structurally closer to the genuine DNA molecule composition. In its structure, thymidine is a joint of deoxyribose (a pentose sugar) with the pyrimidine base thymine (the thymidine molecular structure can be seen in ball-and-stick mode in the inset of Figure 1a). We investigate the self-assembled behavior of TD molecules on Au(111) and make comparisons with that of thymine on the same surface.²⁸ In addition, a novel phase is probed, namely, the parallel-line structure. The phase transition from the dimer structure to this parallel-line structure is also observed by STM. On the basis of our experimental observations and theoretical calculations, we further reveal the role of the deoxyribose group in the intermolecular interactions and the self-assembly process.

Experimental Methods

The experiments were conducted in an ultrahigh vacuum (UHV) system equipped with molecular evaporators and variable temperature scanning tunneling microscopy (VT-STM) (OMI-CRON, Germany). The Au(111) substrate was cleaned first in an ultrasonic bath of acetone, then ethanol, and then water before transferring into the UHV chamber with a base pressure of $\sim 2 \times 10^{-10}$ mbar. The clean Au(111) surface with wide terraces covered by the herringbone reconstruction was obtained after several cycles of Ar⁺ sputtering and annealing (750 K) under

* To whom correspondence should be addressed. E-mail: hjgao@aphy.iphy.ac.cn.

[†] Institute of Physics.

[‡] Institute of Chemistry.

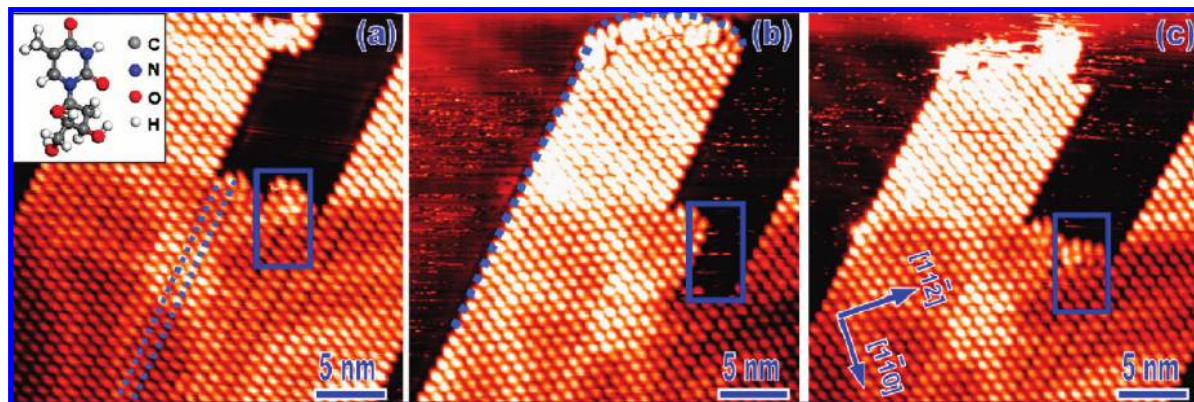


Figure 1. A series of STM images of TD islands consisting of dimer chains at submonolayer coverage. The sample is kept at room temperature during the preparation and measurement process. All images are obtained with the scanning parameters $V = -1.29$ V and $I = 0.10$ nA. The rectangle marks the moving dimer chains. The fuzzy noise around the molecular island indicates the fast diffusion of TD molecules at RT.

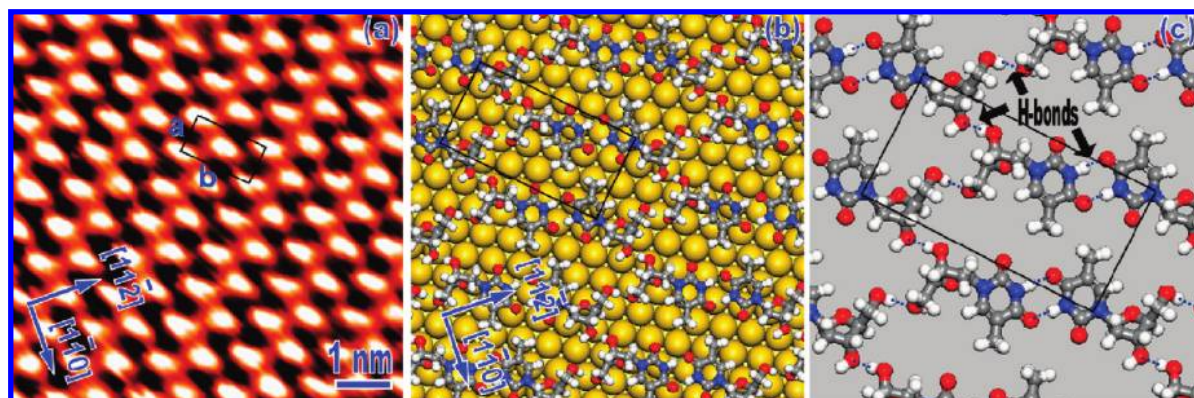


Figure 2. (a) Zoom-in STM image of the TD dimer chain islands; $V = -1.16$ V, $I = 0.10$ nA. (b and c) Calculated molecular models of TD dimer structures. The parallelogram marks the unit cell of the molecular superlattice. The dashed lines depict the intermolecular H-bondings.

UHV conditions. Thymidine (from Sigma) was purified by thermal evaporation at HV conditions (10^{-7} mbar) before being put into the UHV chamber. It was further degassed for 12 h under UHV conditions and afterward deposited onto Au(111) surface by organic molecular beam epitaxy. The structure and morphology of TD on Au(111) were measured by STM, at both room temperature and 100 K. The scanning tip was made of tungsten wire by electrochemical etching.

Results and Discussion

Figure 1 shows typical STM images of the self-assembled TD islands at room temperature (RT). In the images, the herringbone feature of the Au(111) surface can clearly be seen underneath the molecular islands. This suggests that the adsorbate–substrate interaction is laterally flat and the TD molecules are not strongly confined by the reconstructed herringbone stripes. Focusing in Figure 1a, the TD islands apparently consist of parallel dimer chains, as indicated by dotted lines. The lateral size of one protrusion is about 0.6 nm, which is in accordance with the molecular size and thus represents one single TD molecule. It should be noted that the fuzzy features observed on the bare Au(111) surface near the islands probably originate from fast-moving molecules. This implies that a fraction of the molecules is in a gas-like state and diffuses quickly on the Au(111) surface. Fast quenching to low temperature (100 K) leads to disordered molecular patches, attached to the boundaries of the ordered islands. A similar glassy system has recently been addressed for cytosine,³¹ another NB molecule. In addition, the different STM snapshots shown in Figure 1 are obtained by consecutive scanning of the same area. We note

that a section of the molecular island is missing from Figure 1a and b (marked by the blue rectangle), and later comes back in Figure 1c. This indicates that the gas-like phase undergoes frequent solidification/gasification processes at the edge of the molecular island under STM scanning.

Figure 2a presents the zoom-in STM image of the molecular islands. Two neighboring protrusions compose a dimer, and the neighboring dimers form straight chains aligning with a rotation angle of 15° with respect to $[1\bar{1}0]$ direction of the Au(111) substrate. The alternative bright and dark stripes between molecular chains clearly prove the dimer structure. The unit cell of the molecular superlattice is also given in the image. The corresponding matrix to Au(111) can be described as

$$\begin{pmatrix} 7 & 5 \\ 1 & 4 \end{pmatrix}$$

with the parameters of $a = 0.88 \pm 0.02$ nm and $b = 1.76 \pm 0.04$ nm, with the angle between a and b of $90^\circ \pm 2^\circ$.

To understand this structure, we conducted density functional theory (DFT) calculations with the Vienna ab initio simulation package (VASP)²⁹ to optimize structural models. The Perdew–Burke–Ernzerhof (PBE)³⁰ exchange–correlation potential was used, and optimized structures were obtained until the force change for each atom was less than 0.02 eV/Å. The substrate was constructed by four layers of gold atoms, with the bottom two layers fixed. The gold slabs were separated by a 16 Å vacuum layer in the direction orthogonal to the surface. The cutoff energy for plane waves was 400 eV. For k -point sampling

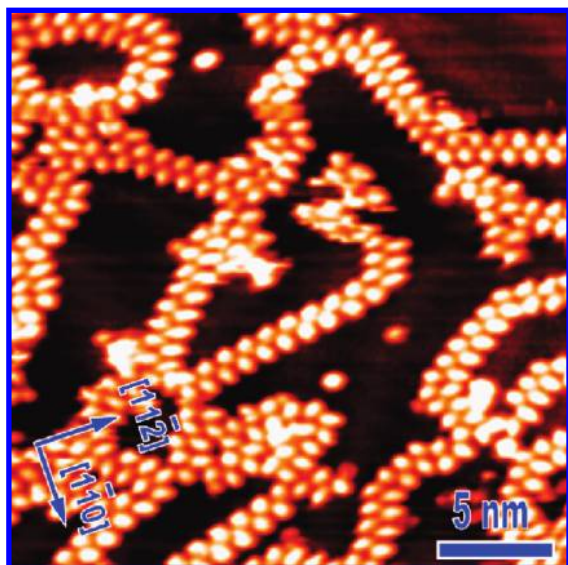


Figure 3. Low-temperature STM image (100 K) displaying the dispersed filament structure of the TD dimer. The sample was prepared by keeping the substrate at 150 K.

of the Brillouin zone, we used the $1 \times 1 \times 1$ Monkhorst–Pack grid. The optimized dimer structure is presented in Figure 2b. Noting that the adsorbate–substrate interaction is laterally flat, we hereby ascribe the ordered superstructure to the intermolecular hydrogen bonds. As depicted in Figure 2c, the face-to-face nucleic acid base groups are paired by two N–H \cdots O=R hydrogen bonds and then tied together by O–H \cdots O–R hydrogen bonds via deoxyribose moieties. Due to the different strengths of these two types of hydrogen bonds, the dimer structure arises. To evaluate the roles of these two kinds of H-bonds in the formation of the ordered structure, we calculate the binding energy with the method of Gaussian (B3LYP/6-31G*, with basis set superposition error (BSSE) correction).³² The binding energies of thymine dimers and deoxyribose dimers are about 0.81 and 0.35 eV, respectively. The data are similar to the values (0.86 and 0.36 eV, respectively) based on VASP method. This indicates that TD molecules bind more tightly at the pyrimidine site. Furthermore, the different strength also accounts for the anisotropy of the elongated shape of TD islands. As can be seen in Figure 1b, the edge of the molecular island along the chain direction (deoxyribose-terminated side) is perfectly straight, as depicted by the dashed line, while the other edge (pyrimidine-terminated side) is irregular. Due to the higher binding energy of N–H \cdots O=R groups, extra molecules prefer to attach to the pyrimidine-terminated side, which causes the formation of the rough edge.

Low-temperature experiments were also conducted. We prepared the sample at a substrate temperature of 150 K and then quickly transferred it to the STM measurement stage, which was precooled to 100 K. Figure 3 shows a typical STM image obtained at low temperature. TD molecules form dimer filaments spreading on the surface. The overall distribution of the filaments is irregular and shows no long-range order. Temperature-rising experiments demonstrate that TD filaments start to aggregate into ordered islands after increasing the sample temperature above ~ 250 K. All data suggest that the TD filament structure at low temperature is a metastable phase caused by insufficient thermal activation. Besides, it also reveals that the interaction within a dimer chain is stronger than that between the chains.

Compared with thymine,²⁸ we find that the joint of the deoxyribose moiety leads to different chemical and physical

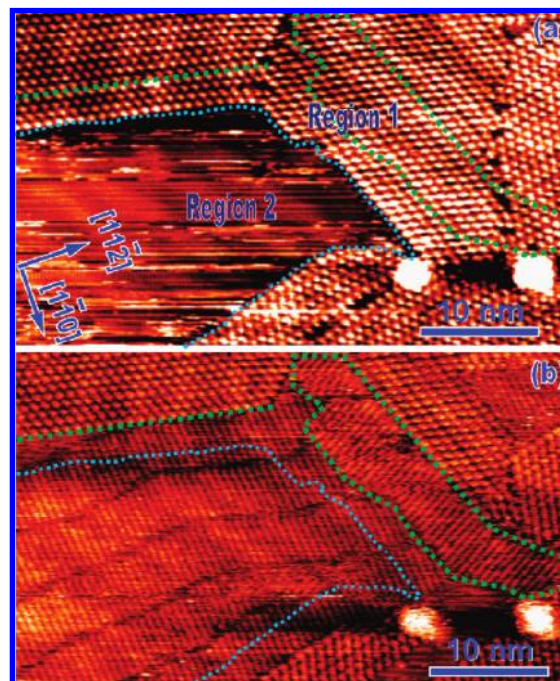


Figure 4. Room-temperature STM snapshots of the sample obtained at the same area; $V = -1.26$ V, $I = 0.10$ nA. The fast diffusing gas-like phase (Region 2) and the dimer chains (Region 1) both transform to parallel-line structures induced by a STM-stimulated process.

behavior of TD in many aspects. Specifically, thymine molecules form irregular filaments at RT at low coverage, and ordered islands can only be obtained when the coverage increases. Manipulations via STM voltage pulse (ramping from 1 to 10 V) disassemble the thymine islands into filaments, which suggest that only weak van der Waals interactions interconnect the filaments. In contrast, however, for TD molecules in our experiments, the filaments aggregate to large islands at RT. Dispersed filaments were not achieved until we cooled down the substrate below 100 K during deposition to reduce the molecular diffusion. In addition, well-ordered TD islands can be observed at small molecular coverage, and the voltage pulses do not take the TD islands apart. The formation of large molecular islands rather than dispersed filaments at RT suggests a stronger intermolecular interaction between the TD filaments than that between those of thymine. The stability of the TD islands under STM voltage pulses also proves the strong intermolecular interactions. TD molecules combine into dimer chains due to the great number of H-bonds via the sugar moiety rather than weak van der Waals interactions, which accounts for all of these discrepancies.

Under consecutive STM scanning, a novel phase with a parallel-line arrangement can be observed to develop gradually among dimer domains. Figure 4a and b presents typical STM images before and after the formation of the parallel-line structure. Two bright spots at the bottom of the images can serve as references. Figure 4a shows the dimer islands as well as the bare surface with diffusing gas-like TD. After several cycles of scanning, the parallel-line structure gradually appears, as shown in Figure 4b. Comparing these two images, we note that the previous bare surface is now fully covered with the molecular lines (e.g., Region 1), and some dimer chains near the domain edge also undergo the transformation into parallel lines (e.g., Region 2). This suggests that the fast-diffusing gas-like phase as well as the dimer phase can transform into the TD parallel-line structure. Considering the driving force of the phase

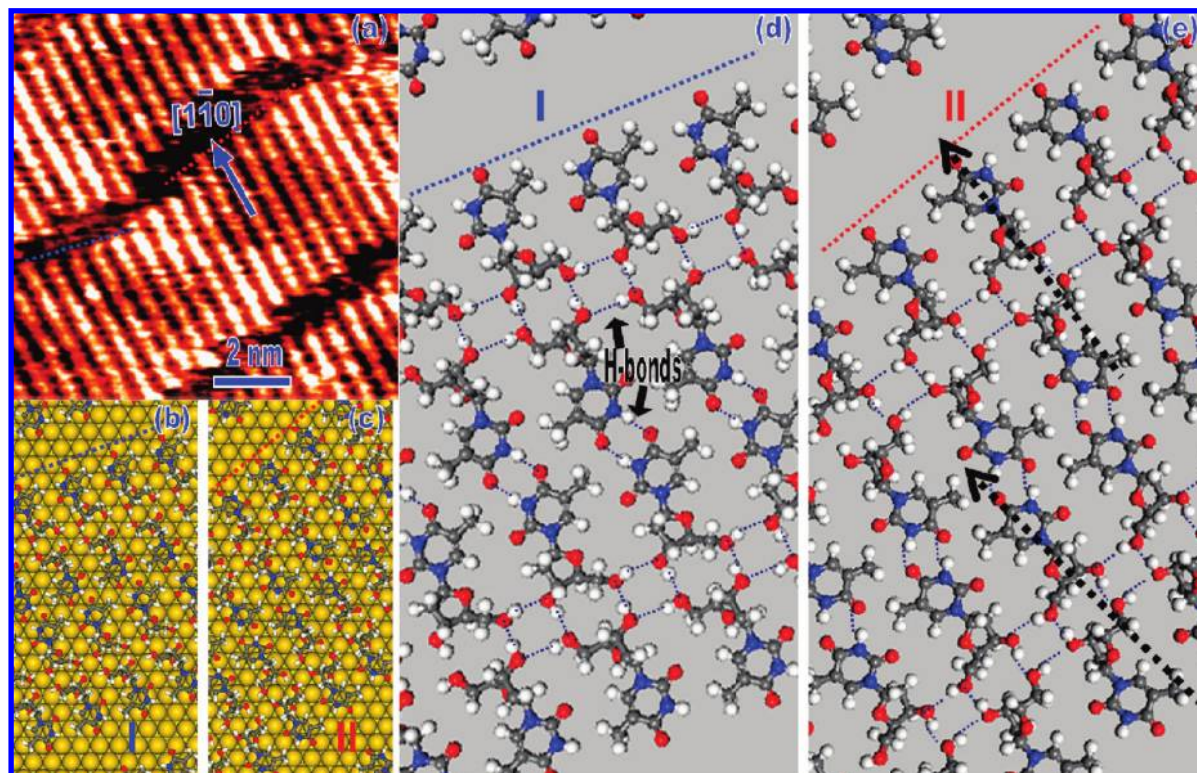


Figure 5. (a) Typical close-up STM image of a parallel-line structure; $V = -1.26$ V, $I = 0.10$ nA. All molecular lines align along equivalent $[1\bar{1}0]$ directions of the substrate. (b and c) Calculated molecular models of the parallel-line structure with two chiral conformations (denoted as I and II, respectively). (d and e) Different directions of the edges of the molecular arrays, consisting of two chiral conformations of TD molecules. The black dashed lines in (e) display the rotation of TD molecules, which geometrically hinders the formation of continuous TD molecular lines. The short dashed lines in (d) and (e) depict the intermolecular H-bondings.

transition, the electron injection from the tunneling current may possibly stimulate this phase transition when the tip scans over the surface. Since this structure has not been reported for the thymine case, thus, we regard it as a unique phase of TD, which is apparently induced by the joint of the deoxyribose moiety, as analyzed below.

As shown in the zoom-in STM image of this line structure in Figure 5a, most of these lines align along the three equivalent $[1\bar{1}0]$ directions of the Au(111) surface, and the distance between neighboring lines is about 0.57 ± 0.03 nm, more compact than the dimer structure. It should be also noted that the length of these lines has a fixed value, on average, about 4.2 ± 0.1 nm. Here, the measured superlattice of the parallel-line structure is incommensurate. Thus, we conduct the DFT calculations with a slightly bigger but commensurate unit cell. Figure 5b presents the optimized structure (for the k -points sampling, a $2 \times 1 \times 1$ Monkhorst–Pack grid is used here). Each line contains four molecules. Deoxyribose groups play a crucial role in this conformation. Two TD molecules are tightly combined together via $O-H\cdots O-R$ bonds of the sugar moiety and then linked together, forming two pairs of $N-H\cdots O=R$ bonds via the thymine moiety, which result in the linear alignment observed in the STM. Additionally, every two lines are bonded by four pairs of $O-H\cdots O-R$ bonds (see Figure 5d and e), which leads to the compact array. Due to bonding constraints, the orientation of the thymine moiety of the TD molecule at the end has an 8° rotation with respect to the one in the middle, indicated by the black dashed line in Figure 5e. In this way, if one more molecule is attached to the end of the line in order to form the periodic structure, there will be a 16° relative rotation between the two thymine moieties. As a consequence, any stable hydrogen bond between an attached

molecule and the edge one is geometrically forbidden, and each line can only contain four molecules. The length is thus about 4.0 nm, close to the measured STM value (4.2 ± 0.1 nm).

Besides, due to molecular chirality, there are two chiral conformations, I and II, respectively, as depicted in Figure 5b and c. Although in both conformations molecular lines align along the same $[1\bar{1}0]$ direction (the mirror-symmetric axis), the lateral arrangement differs. This thus results in the undulated edges of the molecular arrays. As illustrated by dashed lines in Figure 5a, two differently oriented edges are correspondingly observed, rotating $\pm 80^\circ$ respect to $[1\bar{1}0]$ direction. We hereby conclude that the undulated molecular array of this line structure is a mixture of both chiral species, and the proportion shows no obvious predominance.

By counting the H-bonds of both phases, the line structure obviously overwhelms the dimer one. Besides, DFT calculations also show that the bonding energies per molecule in the molecule layer (without substrate) are 0.58 and 0.61 eV for the dimer and line conformation, respectively. Meanwhile, from the experimental point of view, the reverse transition, that is, from the line into the dimer structure, has never been found. This fact further convinces that the line structure is more energetically favorable. However, these molecular lines cannot spontaneously form at RT. This thus suggests some energy barrier between the two states, which blocks this phase transition. When conducting the STM scanning on the molecular film, the energy introduced by the tunneling current assists the TD molecules to cross over the barrier and transform into the line structure. To confirm our speculations, we cooled down the sample to 100 K, and the line structure could not be triggered any more. This demonstrates that the molecules are thermally less activated

at low temperature and the transition barrier cannot be overcome by the electron injection anymore.

Conclusions

The growth of thymidine on Au(111) was investigated by UHV-STM. At room temperature, TD molecules prefer to form dimer chains that further aggregate into islands. The fuzzy STM images suggest that free TD molecules rapidly diffuse on the surface in a gas-like phase, and these molecules can be attached to the existing dimer structure. We compared the experimental data to the previous work with thymine on the Au(111) surface and found that the deoxyribose group of TD molecules has a strong influence on the self-assembly behavior of DNA nucleic acid bases. Deoxyribose groups remarkably enhance the intermolecular interaction and stabilize the self-assembled dimer structures even at low temperature.

In addition, the deoxyribose groups were mainly responsible for the formation of a phase with a parallel-line structure, which can be observed to develop among dimer domains at RT under consecutive scanning. Careful examination of the transition process reveals that these molecular lines can be transformed from both the gas-like and dimer phase when the molecules are driven past the transition barrier by tunneling current stimulation. The phase transition cannot be achieved after cooling down to 100 K.

Acknowledgment. We acknowledge K. H. Rieder and N. Nilius for fruitful discussions. The work was supported by the National Science Foundation of China (Grants 10674159 and 10874219), '863' and '973' projects, as well as the Supercomputing Center, CNIC, in China.

References and Notes

- (1) Watson, J. D.; Crick, H. C. *Nature* **1953**, *171*, 737.
- (2) Chen, Q.; Richardson, N. V. *Nat. Mater.* **2003**, *2*, 324–328.
- (3) Binnig, G.; Rohrer, H.; Gerber, C. H.; Weibel, E. *Phys. Rev. Lett.* **1983**, *50*, 120.
- (4) Camargo, A. P. M.; Baumgartel, H.; Donner, C. *Phys. Chem. Commun.* **2002**, *5*, 151–157.
- (5) Roelfs, B.; Bunge, E.; Schroter, C.; Solomun, T.; Meyer, H.; Nichols, R. J.; Baumgartel, H. *J. Phys. Chem. B* **1997**, *101*, 754–765.
- (6) Li, W. H.; Haiss, W.; Floate, S.; Nichols, R. J. *Langmuir* **1999**, *15*, 4875–4883.
- (7) Dretschkow, T.; Dakkouri, A. S.; Wandlowski, T. *Langmuir* **1997**, *13*, 2843–2856.
- (8) Avci, E.; Meyer, C.; Donner, C. *J. Electroanal. Chem.* **2006**, *589*, 24–31.
- (9) Weightman, P.; Dolan, G. J.; Smith, C. I.; Cuquerella, M. C.; Almond, N. J.; Farrell, T.; Fernig, D. G.; Edwards, C.; Martin, D. S. *Phys. Rev. Lett.* **2006**, *96*, 4.

- (10) Sowerby, S. J.; Petersen, G. B. *J. Electroanal. Chem.* **1997**, *433*, 85–90.
- (11) Cunha, F.; Sa, E.; Nart, F. *Surf. Sci.* **2001**, *480*, L383–L388.
- (12) Tao, N. J.; Derosé, J. A.; Lindsay, S. M. *J. Phys. Chem.* **1993**, *97*, 910–919.
- (13) Holzle, M. H.; Wandlowski, T.; Kolb, D. M. *Surf. Sci.* **1995**, *335*, 281–290.
- (14) Mamdouh, W.; Dong, M. D.; Xu, S. L.; Rauls, E.; Besenbacher, F. *J. Am. Chem. Soc.* **2006**, *128*, 13305–13311.
- (15) Boland, T.; Ratner, B. D. *Langmuir* **1994**, *10*, 3845–3852.
- (16) Yamada, T.; Shirasaka, K.; Takano, A.; Kawai, M. *Surf. Sci.* **2004**, *561*, 233–247.
- (17) Frankel, D. J.; Chen, Q.; Richardson, N. V. *J. Chem. Phys.* **2006**, *124*.
- (18) Otero, R.; Schock, M.; Molina, L. M.; Laegsgaard, E.; Stensgaard, I.; Hammer, B.; Besenbacher, F. *Angew. Chem., Int. Ed.* **2005**, *44*, 2270–2275.
- (19) Chen, Q.; Frankel, D. J.; Richardson, N. V. *Langmuir* **2002**, *18*, 3219–3225.
- (20) Plekan, O.; Feyer, V.; Sutara, F.; Skala, T.; Svec, M.; Chab, V.; Matolin, V.; Prince, K. C. *Surf. Sci.* **2007**, *601*, 1973–1980.
- (21) Kelly, R. E. A.; Xu, W.; Lukas, M.; Otero, R.; Mura, M.; Lee, Y. J.; Laegsgaard, E.; Stensgaard, I.; Kantorovich, L. N.; Besenbacher, F. *Small* **2008**, *4*, 1494–1500.
- (22) Spöner, J.; Jurecka, P.; Hobza, P. *J. Am. Chem. Soc.* **2004**, *126*, 10142–10151.
- (23) Kelly, R. E. A.; Kantorovich, L. N. *J. Phys. Chem. B* **2006**, *110*, 2249–2255.
- (24) Edelwirth, M.; Freund, J.; Sowerby, S. J.; Heckl, W. M. *Surf. Sci.* **1998**, *417*, 201–209.
- (25) Sowerby, S. J.; Edelwirth, M.; Heckl, W. M. *J. Phys. Chem. B* **1998**, *102*, 5914–5922.
- (26) Piana, S.; Bilic, A. *J. Phys. Chem. B* **2006**, *110*, 23467–23471.
- (27) Gowtham, S.; Scheicher, R. H.; Ahuja, R.; Pandey, R.; Karna, S. P. *Phys. Rev. B* **2007**, *76*, 4.
- (28) Xu, W.; Kelly, R. E. A.; Otero, R.; Schock, M.; Laegsgaard, E.; Stensgaard, I.; Kantorovich, L. N.; Besenbacher, F. *Small* **2007**, *3*, 2011–2014.
- (29) Kresse, G.; Furthmüller, J. *Phys. Rev. B* **1996**, *54*, 11169–11186.
- (30) Perdew, J. P.; Burke, K.; Ernzerhof, M. *Phys. Rev. Lett.* **1996**, *77*, 3865–3868.
- (31) Otero, R.; Lukas, M.; Kelly, R. E. A.; Xu, W.; Laegsgaard, E.; Stensgaard, I.; Kantorovich, L. N.; Besenbacher, F. *Science* **2008**, *319*, 312–315.
- (32) Frisch, M. J.; Trucks, G. W.; Schlegel, H. B.; Scuseria, G. E.; Robb, M. A.; Cheeseman, J. R.; Montgomery, J. A., Jr.; Vreven, T.; Kudin, K. N.; Burant, J. C.; Millam, J. M.; Iyengar, S. S.; Tomasi, J.; Barone, V.; Mennucci, B.; Cossi, M.; Scalmani, G.; Rega, N.; Petersson, G. A.; Nakatsuji, H.; Hada, M.; Ehara, M.; Toyota, K.; Fukuda, R.; Hasegawa, J.; Ishida, M.; Nakajima, T.; Honda, Y.; Kitao, O.; Nakai, H.; Klene, M.; Li, X.; Knox, J. E.; Hratchian, H. P.; Cross, J. B.; Bakken, V.; Adamo, C.; Jaramillo, J.; Gomperts, R.; Stratmann, R. E.; Yazyev, O.; Austin, A. J.; Cammi, R.; Pomelli, C.; Ochterski, J. W.; Ayala, P. Y.; Morokuma, K.; Voth, G. A.; Salvador, P.; Dannenberg, J. J.; Zakrzewski, V. G.; Dapprich, S.; Daniels, A. D.; Strain, M. C.; Farkas, O.; Malick, D. K.; Rabuck, A. D.; Raghavachari, K.; Foresman, J. B.; Ortiz, J. V.; Cui, Q.; Baboul, A. G.; Clifford, S.; Cioslowski, J.; Stefanov, B. B.; Liu, G.; Liashenko, A.; Piskorz, P.; Komaromi, I.; Martin, R. L.; Fox, D. J.; Keith, T.; Al-Laham, M. A.; Peng, C. Y.; Nanayakkara, A.; Challacombe, M.; Gill, P. M. W.; Johnson, B.; Chen, W.; Wong, M. W.; Gonzalez, C.; Pople, J. A. *Gaussian 03*, revision E.01; Gaussian, Inc.: Wallingford, CT, 2004.

JP906944C